Three-Dimensional Discrete Heterogeneous Finite Element Method and Code for Static Multi-Group Neutron Diffusion

E. Aydogdu and E. Nichita
University of Ontario Institute of Technology, Oshawa, Ontario, Canada

Abstract

Accurate prediction of the neutron flux and power at the fuel pin level rather than at the fuel-assembly level requires, in principle, lengthy many-group transport-theory calculations using a detailed (fuel-pin level) geometrical representation of the core. Many-group fine-mesh diffusion theory, in conjunction with advanced fuel-pin-cell homogenization techniques, can also be used successfully to predict individual fuel pin powers but the computational effort is still sizeable because of the many regions and groups involved. A three dimensional diffusion code was developed which reduces the time taken by such full-core fine-mesh fine-group diffusion calculations by applying the finite-element method to the discrete form of the many-group fine-mesh diffusion equation and thus reducing the number of unknowns. Preliminary tests performed on a highly-heterogeneous three dimensional three-group model found the code to produce pin power results with a maximum error of 3.5% of the maximum pin power value, with an eight-fold reduction in computational time compared to a regular full-core fine-mesh calculation.

1. Introduction

Finding the neutron flux in the entire core of a nuclear power reactor is a challenging computational problem because of the large size and strong heterogeneity of the reactor core. The general problem of finding the neutron flux is most accurately addressed in multi-group transport theory using fine energy groups (100-300 groups) and a detailed geometrical representation of the core where each fuel pin is represented as a separate region. Various methods exist for discretizing the transport equation in angle, energy, and space. All of them, however, are computationally intensive and therefore only practical for smaller-size problems (usually bi-dimensional representations of a fuel assembly/bundle and the moderator surrounding it), but not for the entire reactor core.

To reduce the size of the problem, full-core calculations are usually performed in diffusion theory and for an approximate geometrical representation of the core obtained by homogenizing the neutronic properties over relatively large, fuel-assembly-size, sub-domains, and condensing them into few (usually two) coarse energy groups. What this means in practice is that full-core codes used for day-to-day design can provide average quantities over entire fuel assemblies (bundles) but not values for individual fuel pins. The fuel-pin level quantities can be reconstructed from assembly-average quantities using various approximate methods.

It is still possible to obtain fuel-pin-level flux and power distributions directly from diffusion theory calculations if pin-level rather than assembly-level homogenization is performed and if fine group energy discretization is used. To ensure diffusion-theory results are close to transport results, homogenization and group condensation have to be performed using some advanced homogenization technique, such as superhomogenization [1]. Such diffusion calculations are still time consuming because of the large number of spatial regions and many energy groups involved.

The work presented here reduces the time taken by such full-core fine-mesh fine-group diffusion calculations by applying the finite-element method to the discrete form of the multigroup diffusion equation and thus reducing the number of unknowns.

2. General approach

The Discrete Heterogeneous Finite Element Method (DHFEM) presented here follows the outline of the usual (continuous, homogeneous) Finite Element Method (FEM), but starts from the fine-group, fine-mesh, mesh-centered finite-difference form of the diffusion equation, written in operator form as:

$$\mathbf{M}\,\Phi = \frac{1}{k_{eff}}\mathbf{F}\,\Phi \qquad \textbf{(1)}$$

In Eq. (1), $\Phi = \Phi(i,j,k,g)$ represents the flux vector whose elements are the flux in fine-group g at the center of Cartesian fine-mesh box (i,j,k). $\mathbf{M}$ and $\mathbf{F}$ represent the fine-group fine-mesh discrete forms of the loss operator and production operator defined, using standard notations, as:

$$[\mathbf{M}\,\Phi](i,j,k,g) \equiv -[\mathbf{L}\,\Phi](i,j,k,g) + \Sigma_t(i,j,k,g)\Phi(i,j,k,g) - \sum_{g'=1}^{N_g}\Sigma_s(i,j,k,g' \to g)\Phi(i,j,k,g') \qquad \textbf{(2)}$$

$$[\mathbf{F}\,\Phi](i,j,k,g) \equiv \chi(i,j,k,g)\sum_{g'=1}^{N_g} \nu\Sigma_f(i,j,k,g')\Phi(i,j,k,g') \qquad \textbf{(3)}$$

The leakage operator, $\mathbf{L}$, is defined as the sum of the leakage in all directions:

$$[\mathbf{L}\,\Phi](i,j,k,g) = [\mathbf{L}_x\,\Phi](i,j,k,g) + [\mathbf{L}_y\,\Phi](i,j,k,g) + [\mathbf{L}_z\,\Phi](i,j,k,g) \qquad \textbf{(4)}$$

The directional leakage operator for the x direction, $\mathbf{L}_x$, is defined as [2]:

$$[\mathbf{L}_x\,\Phi](i,j,k,g) \equiv \frac{D(i,j,k,g)}{h_{x,i}}\left[\frac{2D(i+1,j,k,g)[\Phi(i+1,j,k,g)-\Phi(i,j,k,g)]}{h_{x,i+1}D(i,j,k,g)+h_{x,i}D(i+1,j,k,g)} - \frac{2D(i-1,j,k,g)[\Phi(i,j,k,g)-\Phi(i-1,j,k,g)]}{h_{x,i}D(i-1,j,k,g)+h_{x,i-1}D(i,j,k,g)}\right] \qquad \textbf{(5)}$$

$\mathbf{L}_y$ and $\mathbf{L}_z$ are defined analogously.

In the above equation, h_x, h_y *and* h_z represent the fine-mesh size in each direction. The DHFEM method proceeds by dividing the volume of the reactor into large parallelepiped-shaped elements. The element corners are called nodes. Each element is, in turn, subdivided into Cartesian subregions, each subregion corresponding to one fine-mesh box of the finite-difference grid, indexed by the triplet (i,j,k). Normally, an element is chosen to encompass a fuel assembly in the x-y plane and extend approximately 0.5m in the Z direction. A sub-region is usually chosen to consist of a homogenized fuel-pin cell (pin plus coolant) or of pure moderator/coolant. The actual choice of elements and subregions is flexible and depends on the configuration being analyzed. The energy is divided first into coarse groups, indexed by *G*. Coarse groups are, in turn, subdivided into

fine groups indexed by *g*. The fine-group structure is the same as in the finite-difference discretization used in Eq. (2). A representation of the core sub-division into elements and subregions is shown in Fig. 1.

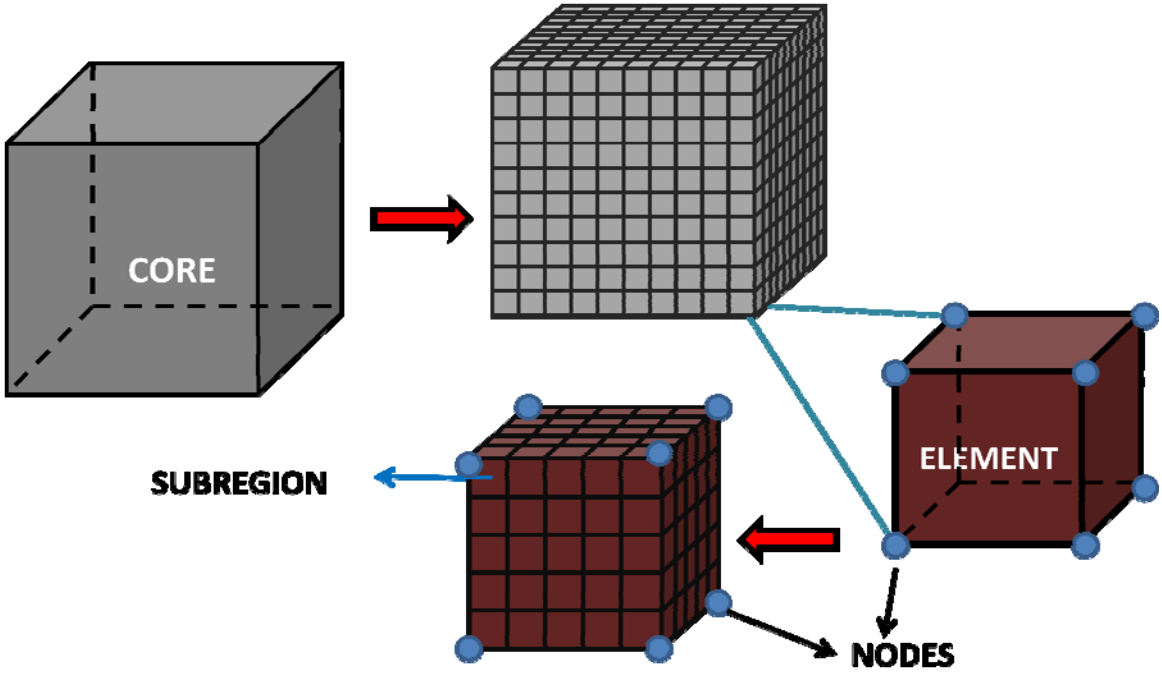

Figure 1: Elements, nodes and subregions for a three-dimensional geometry

The solution of the discretized multi-group diffusion equations is sought as a linear combination of discrete basis (trial) functions of space and energy, one for each node and coarse energy group:

$$\Phi(i,j,k,g) = \sum_{G} \sum_{n} \phi_{n,G}\, \psi_{n,G}(i,j,k,g) \qquad \textbf{(6)}$$

In Eq. (6) $\psi_{n,G}(i,j,k,g)$ is the (discrete) basis function corresponding to node *n* and coarse energy-group *G*. $\phi_{n,G}$ are the expansion coefficients which are to be determined.

The basis function $\psi_{n,G,}(i,j,k,g)$ is defined as a sum of eight elementary basis functions, $\varphi_{n,G,e}$, each of which is nonzero only in one of the eight elements surrounding the node *n* and only for fine groups *g* belonging to coarse group *G*.

$$\psi_{n,G}(i,j,k,g) = \sum_{e \in (\text{neighbors of n})} \varphi_{n,G,e}(i,j,k,g) \qquad \textbf{(7)}$$

Each basis function can be regarded as consisting of eight elementary basis functions "glued" together at the common node. Consequently, each elementary basis function $\varphi_{n,G,e}$ can be regarded

as a "branch" of the basis function $\psi_{n,G}$ which is non-zero only inside a single neighbouring element *e* and for fine groups *g* belonging to coarse group *G*.

In analogy to the regular FEM, each discrete elementary basis function $\varphi_{n,G,e}$ is constructed such that the energy integral of its continuous counterpart is equal to one at node *n* defined by its coordinates (x_n, y_n, z_n):

$$\sum_{g\in G} \varphi_{n,G,e}(x_n, y_n, z_n, g) = 1 \qquad \textbf{(8)}$$

and it vanishes at all the remaining seven nodes (corners) of element *e*. Consequently, each of the coefficients $\phi_{n,G}$ represents the amplitude of the flux in coarse group *G*, at node *n*.

In general, the choice of basis (trial) functions depends on the problem that needs to be solved.

Substituting Eq. (7) into the finite-difference-discretized diffusion equation the following is obtained:

$$\sum_G \sum_n \phi_{n,G} \left[\mathbf{M}\,\psi_{n,G}\right](i,j,k,g) = \frac{1}{k} \sum_G \sum_n \phi_{n,G} \left[\mathbf{F}\,\psi_{n,G}\right](i,j,k,g) \qquad \textbf{(9)}$$

Next, just as for the regular finite element method, a weighted residual method is applied by taking the inner product of Eq. (9) with weight functions $w_{m,H}(i,j,k,g)$.

The resulting homogeneous linear system is:

$$\sum_G \sum_n \phi_{n,G} \left\langle w_{m,H}; \mathbf{M}\,\psi_{n,G} \right\rangle = \frac{1}{k_{eff}} \sum_G \sum_n \phi_{n,G} \left\langle w_{m,H}; \mathbf{F}\,\psi_{n,G} \right\rangle \qquad \textbf{(10)}$$

The discrete inner product for two arbitrary vectors, Φ and ψ, is defined as:

$$\left\langle \Phi; \psi \right\rangle \equiv \sum_{g,i,j,k} \Phi(i,j,k,g)\,\psi(i,j,k,g)\,h_{x,i}\,h_{y,j}\,h_{z,k} \qquad \textbf{(11)}$$

It will be noted that the inner product defined by Eq. (11) covers both space and energy.

Eq. (10) defines a generalized eigenvalue-eigenvector problem with eigenvalue $\frac{1}{k_{eff}}$ and eigenvector defined by its components $\phi_{n,G}$. It can be rewritten, with obvious notations, as:

$$\sum_G \sum_n M_{n,G}^{m,H} \phi_{n,G} = \frac{1}{k_{eff}} \sum_G \sum_n F_{n,G}^{m,H} \phi_{n,G} \qquad \textbf{(12)}$$

Because each basis function $\psi_{n,G}(i,j,k,g)$ is only non-zero in the eight elements neighbouring node *n* and inside coarse group *G*, the matrices M and F are sparse.

Solution of Eq. (12) proceeds by inverse power iteration. At each inverse power iteration, iterations on the coarse-group scattering source are performed. For each such scattering-source iteration the flux in each coarse group is solved using the Orthomin algorithm. No acceleration techniques are currently used. Once coefficients $\phi_{n,G}$ are found, the fine-mesh fine-energy-group flux is reconstructed using Eq. (6).

The DHFEM allows the basis functions to be chosen such that they capture the fine-mesh detail of the flux distribution. However, the number of unknowns is only of the same order of magnitude as the number of nodes times the number of coarse groups, therefore much smaller than the number of unknowns for a full-core fine-mesh fine-group solution. The DHFEM thus offers fine-mesh and fine group detail at coarse-mesh coarse-group computational cost.

3. Choice of elementary basis functions and weight functions

The choice of elementary basis functions is flexible and has to be made depending on the type of problem to be solved. For the current implementation of the code, each elementary basis function $\varphi_{n,G,e}$ was defined as the product between a (discrete) multivariate polynomial defined in element *e* and the single-element flux shape for element *e*.

$$\varphi_{n,G,e}(i,j,k,g) = \begin{cases} \mathrm{P}_{n,e}(i,j,k)\psi_e^0(g,i,j,k) & g \in G \\ 0 & g \notin G \end{cases} \quad \textbf{(13)}$$

For any node *n* that is a corner of element *e*, the polynomial $\mathrm{P}_{n,e}$ is expressed as:

$$\mathrm{P}_{n,e}(i,j,k) = \left(1 - \frac{|x_i - x_n|}{l_{x,e}}\right)\left(1 - \frac{|y_j - y_n|}{l_{y,e}}\right)\left(1 - \frac{|z_k - z_n|}{l_{z,e}}\right) \quad \textbf{(14)}$$

In Eq. (14) (x_i, y_j, z_k) represent the coordinates of the center of the fine-mesh box (i,j,k), (x_n, y_n, z_n) represent the coordinates of node *n* and $l_{x,e}$, $l_{y,e}$ and $l_{z,e}$ represent the lengths of the sides of element *e*. It can be seen that the (continuous) polynomial defined by Eq. (14) equals one at node *n* and zero at all other seven corners of element *e*. In fact, the polynomial in Eq. (14) vanishes on all three faces of element *e* that are opposite node *n*. Consequently, the elementary basis function defined by Eq. (13) also vanishes on the three element faces opposite the node. In Eq. (13), the single-assembly (single-element) flux shape $\psi_e^0(g,i,j,k)$ is obtained from single-element calculations with reflective boundary conditions and it is normalized so it satisfies Eq. (8). If the element *e* is not symmetric, the normalization may have to be different for each of its corners (nodes) *n*. For the current code implementation, the weight functions were chosen to be equal to the basis functions.

4. Calculations and results

4.1 Test model

For a preliminary test of the code, a simple, yet computationally challenging, model was used. Three energy groups were used for both the fine-group and coarse-group representation. Because the fine- and coarse-group structures are identical, the group-condensation abilities of the DHFEM were not tested with this model. The geometrical model consists of 10 x 10 x 10 elements, each 40

cm x 50 cm x 60 cm in size. Each element is subdivided into 5 x 5 x 5 subregions. The core consists of an inner zone (8 x 8 x 8 elements) made up of "type 2" elements and an outer zone made up of "type 1" elements. Cross-sectional views of the core showing the distribution of element types are displayed in Fig. 2. Each element, regardless of its type, consists of a central region (3 x 3 x 3 sub-regions) and a peripheral region. The peripheral region of "type 1" elements has material properties derived from zero-burnup CANDU fuel-bundle-average cross sections. The peripheral region of "type 2" elements has material properties derived from mid-burnup CANDU fuel-bundle-average cross sections. Material properties of the central regions of both "type 1" and "type 2" elements are identical to those of their respective peripheral regions, with the exception of the thermal (group 3) absorption cross section which is four times higher than its corresponding peripheral absorption cross section. This choice creates a strong heterogeneity in each element, to test the code's ability to capture strong local flux and power variations.

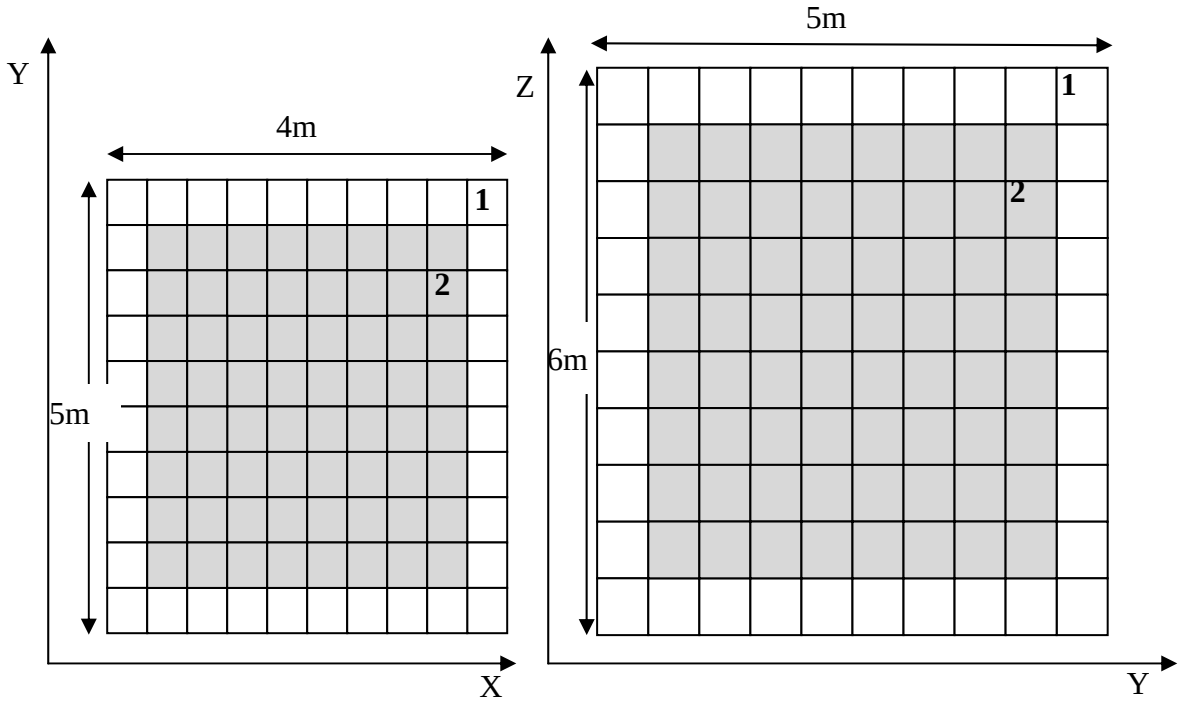

Figure 2: Element-type distribution in the core.

4.2 Results and interpretation

DHFEM results were compared (on a sub-region by sub-region basis) with fine-mesh finite difference results, used as reference, and to regular, homogeneous, FEM results. The latter were obtained by first homogenizing each element and then applying a FEM solution to the element-homogenized model.

The effective multiplication constants and execution times for a 2.13 GHz Intel processor are shown in Table 1. The root mean square percent errors, calculated as:

$$RMSE\% = 100 \cdot \frac{\sum_{i=1}^{N} \left(f_i^{method} - f_i^{ref} \right)^2}{N \cdot \max(f_i)} \qquad \textbf{(15)}$$

are shown in Table 2, together with the error in the effective multiplication constant. The maximum errors as a percent of the maximum value, calculated as

$$MAXE\% = 100 \cdot \frac{\max\left| f_i^{method} - f_i^{ref} \right|}{\max(f_i)} \quad \textbf{(16)}$$

are shown in Table 3.

Finally the maximum local percent errors, calculated as:

$$MAXLE\% = 100 \cdot \max\left(\frac{\left| f_i^{method} - f_i^{ref} \right|}{f_i} \right) \quad \textbf{(17)}$$

are shown in Table 4.

METHOD	k_{eff}	Execution time(min)
Reference	0.72632	30
DHFEM	0.72582	4
FEM	0.72599	4

Table 1: Effective multiplication constant and execution times

METHOD	k_{eff} error (mk)	Φ_1 RMSE%	Φ_2 RMSE%	Φ_3 RMSE%	Power RMSE%
DHFEM	-0.5	0.6	0.6	0.8	0.7
FEM	-0.4	2.9	2.0	7.0	6.5

Table 2: Root mean square percent errors

METHOD	Φ_1 MAXE%	Φ_2 MAXE%	Φ_3 MAXE%	Power MAXE%
DHFEM	2.64	2.69	3.64	3.36
FEM	8.02	5.54	16.30	15.40

Table 3: Maximum percent errors

METHOD	Φ_1 MAXLE%	Φ_2 MAXLE%	Φ_3 MAXLE%	Power MAXLE%
DHFEM	35.2	17.3	68.1	65.3
FEM	32.1	28.9	89.9	87.4

Table 4: Maximum local percent errors

As an example of the code's ability to reproduce fine spatial variations, Fig. 3 shows the power profile along the z axis (variable k) at i=j=23.

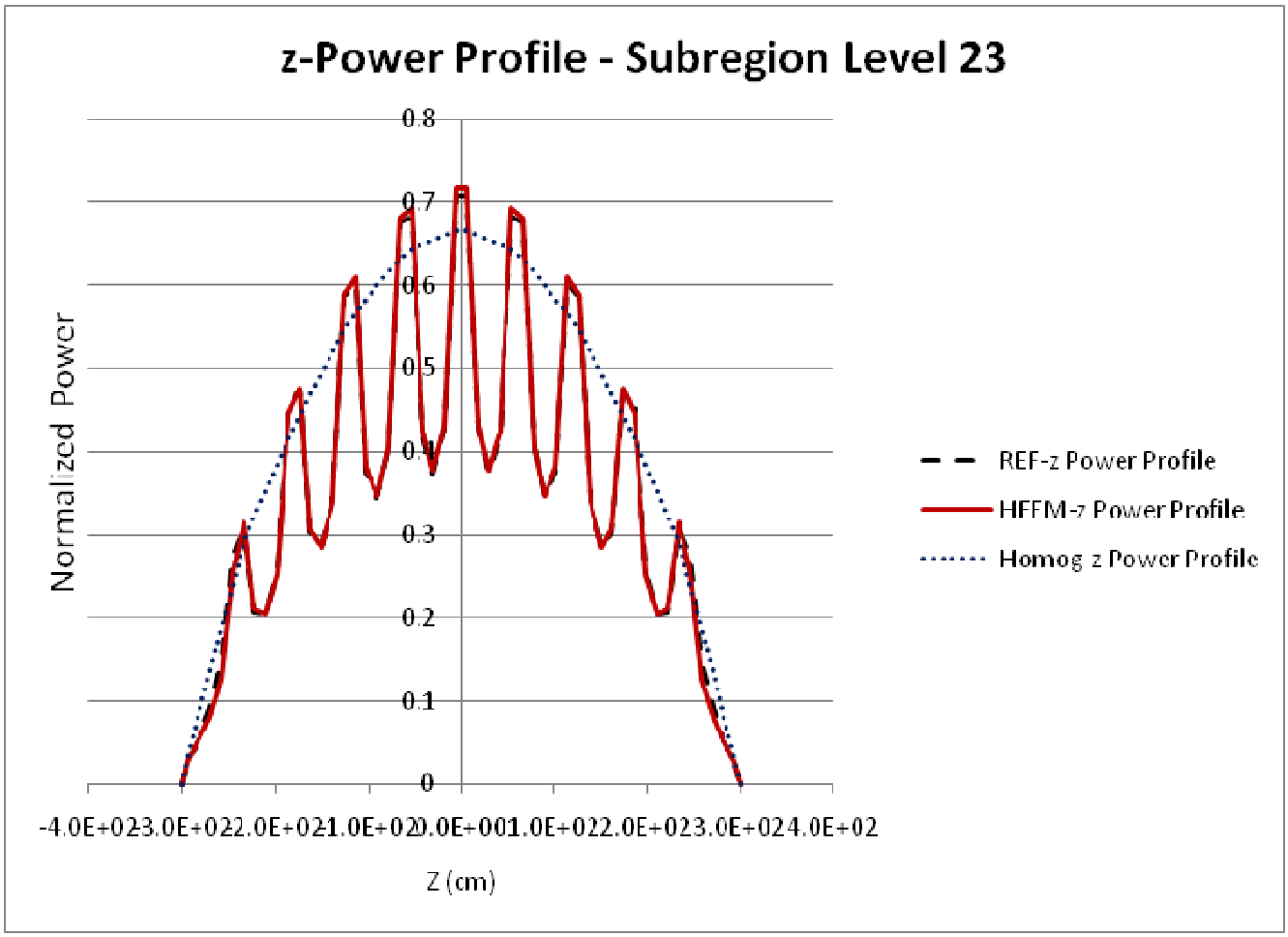

Figure 3: Axial power profile (i=23, j=23, variable k)

Also by way of example, the z profile of the power integrated over each x-y plane, $P_{int}(k) = \sum_{i,j} P(i, j, k)$, is shown in Fig. 4.

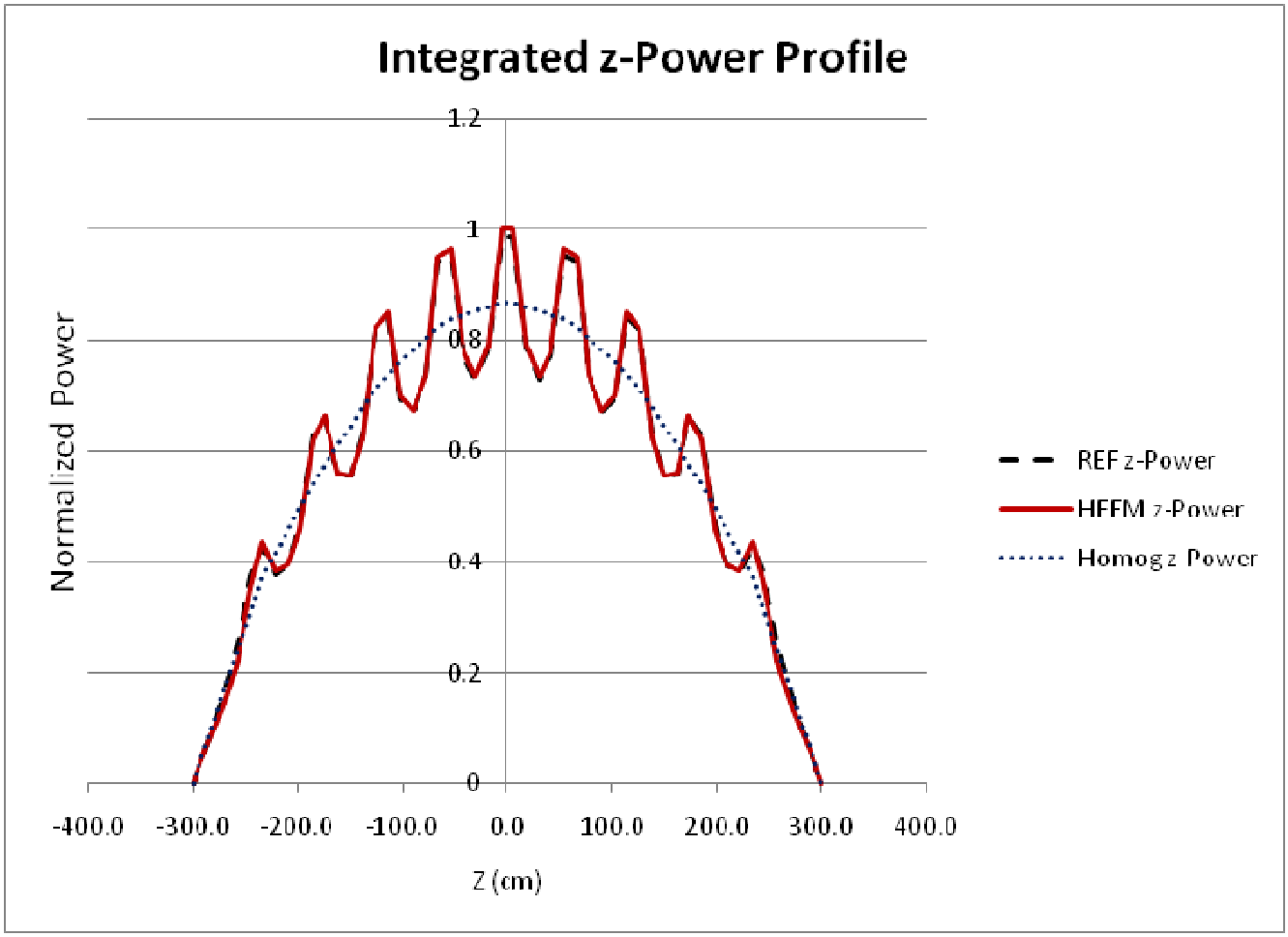

Figure 4: Axial profile of x-y integrated power

Table 1 shows an eight-fold reduction in execution time for the DHFEM compared to the fine-mesh calculation (The number of groups is the same for both methods for the test model that was used.). The somewhat large execution times displayed by all methods can be explained by the absence of any acceleration technique. The reduction in execution time achieved by DHFEM depends, to a large degree, on the number of subregions in each element and on the number of fine groups in each coarse group. In this case, there were 125 subregions in each element. Larger numbers of subregions are expected to yield more substantial reductions in execution time. Similarly, if true fine-group calculations are used for the reference, the reduction in execution time is expected to be more pronounced.

The errors in k_{eff} are similar for the DHFEM and regular FEM and below 1mk. This result is expected since k_{eff} is an integral quantity which depends only weakly on the detailed flux shape. Table 2 shows that, for each energy group, the DHFEM root mean square error is below 1% of the maximum flux value in that group. A similar behaviour is observed for the power. The larger errors for the regular FEM are to be expected since it does not account for fine spatial variations. Table 3 shows that, for all energy groups, maximum errors for DHFEM are below 3.7% of the maximum flux value in that group. The same is true for the power. The large values for the maximum local percent error seen in Table 4 are attained on the periphery of the model, where flux values are very low. Consequently, they are not considered to be a concern. Figures 3 and 4 illustrate graphically the excellent ability of the code to capture fine spatial detail.

5. Conclusion and future investigations

A three-dimensional discrete heterogeneous finite element code was developed which promises to offer accurate values for individual pin powers for the entire core at a computational cost comparable to that of codes using assembly-homogenized core models. Preliminary testing shows that the code is reasonably accurate. Further testing needs to be performed and acceleration techniques need to be investigated and implemented.

6. References

[1] A. Hebert "A Consistent Technique for the Pin-by-Pin Homogenization of a Pressurized Water Reactor Assembly", Nucl. Sci. Eng. 113, 1993, pp. 227-238

[2] E. Nichita, K. Zabienski and M. Gravel, "Three-Dimensional Two-Energy Group Finite-Difference Neutron-Diffusion Code with Discontinuity Factors , Proc. 28th Annual Conference of the Canadian Nuclear Society, Saint John NB, 2007, June 3-6.

[3] R. S. Modak and A. Gupta "New applications of Orthomin algorithm for K-eigenvalue problem in Reactor Physics ", Ann. Nucl. Energy., 33, 2006, pp. 538-543